# Nanoscale

Accepted Manuscript


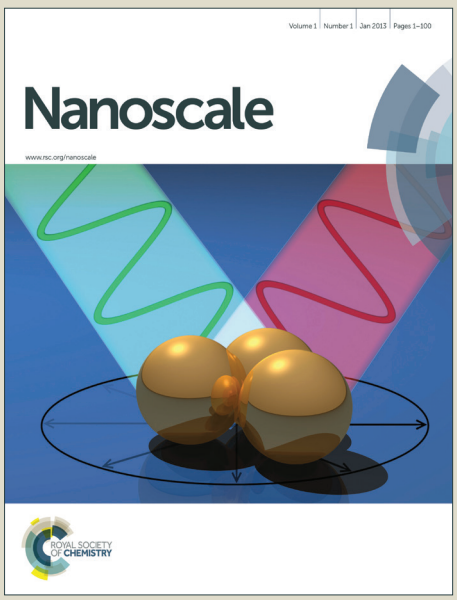





ROYAL SOCIETY OF CHEMISTRY

www.rsc.org/nanoscale

Nanoscale

RSCPublishing

ARTICLE

# Transition from Direct to Fowler-Nordheim Tunneling in Chemically Reduced Graphene Oxide Film

Srikrishna Pandey,[a†] Chandan Biswas,[b†] Titisa Ghosh,[a] Jung Jun Bae,[c] Padmnabh Rai,[d] Gil-Ho Kim,[e] K. J. Thomas,[e] Young Hee Lee,[a] Pavel Nikolaev[a] and Sivaram Arepalli*[a]

Cite this: DOI: 10.1039/x0xx00000x

Received 00th January 2012,
Accepted 00th January 2012

DOI: 10.1039/x0xx00000x

www.rsc.org/

We investigate charge transport in a chemically reduced graphene oxide (RGO) film of sub-micron thickness. The I-V curve of RGO film shows a current switching of the order of ~$10^5$ above a threshold voltage. We found that the observed I-V curve is consistent with quantum tunnelling based charge transport. Quantum tunnelling based Simmons generalized theory has been used to interpret the charge transport mechanism which shows that current switching phenomenon is associated with a transition from direct to Fowler-Nordheim (F-N) tunneling. The absence of current switching in the I-V curve after stripping away the oxygen functional groups from chemically RGO film confirms that the presence of these groups and reduced interaction between adjacent layers of RGO play a key role in charge transport. Such metal-based current switching devices may find applications in graphene-based electronic devices such as high voltage resistive switching devices.



## 1. Introduction

The exceptional and unique combination of the physical, chemical, mechanical and optical properties of graphene exhibit its numerous exotic potential applications in next generation devices.[1-7] Graphene produced by reduction of graphene oxide (GO) provides an excellent way to tailor its properties.[4-5,8-10] Graphene bonded with oxygen-bearing functional groups (mainly epoxy and hydroxyl) producing graphene oxide (GO) exhibits insulating nature due to their disrupted $sp^2$ bonding networks. On the other hand, the reduction of GO leads to re-stabilization of the π-bond network and therefore reduced graphene oxide (RGO) becomes electrical conductive.

The charge transport in individual RGO flake under low bias potential range is consistent with the variable range hopping (VRH) model[11-12] due to the presence of residual impurities and

disorder.[5,7,13-14] However, charge transport in a film of RGO may differ from the individual flake as additional factors such as on the varying number of layers with reduced interlayer interaction, edges, flake to flake interactions etc would be imposed. Moreover charge transport in RGO film at very high bias is expected to show interesting properties above a critical applied voltage due to the presence of insulating functional groups and defects in RGO films. In this article we investigate the charge transport in chemically RGO under a wide range of applied potential.

GO was reduced chemically by a modified method to achieve uniform reduction and to avoid the aggregation of the flakes.[15-16] I-V measurements of RGO film showed dramatically high current switching of the order of ~$10^5$ above a threshold applied voltage. We interpret our data using quantum tunneling based Simmons generalized theory.[17] The current switching in the I-V curve was found to be associated with transition of charge transport from direct to Fowler-Nordheim tunneling. Recently, similar transition of tunneling transport has been observed in some other materials with single tunnel junction.[18-20] Basically the presence of oxygen-bearing functional groups and weak interaction between the flakes/layers play a key role in tunneling based charge transport in RGO, which was confirmed by the subsequent measurements in the absence of functional groups by high temperature annealing. The sharp increase in conductance during high voltage sweep reveals similar switching behavior to a varistor, observed generally in insulating metal oxides or tunnel junctions.[21-23] Observed current switching could be applicable in graphene-based resistive switching devices.

## 2. Experimental

*Chemicals and materials:* All chemicals and materials were purchased from Sigma-Aldrich Company: Graphite flakes, nitric acid, sulfuric acid, hydrochloric acid, potassium chlorate, and hydrazine (35 wt% in water).



 

*Preparation of GO and chemically RGO:* A dispersed graphite oxide suspension in deionized (DI) water was prepared by Staudenmaier method.[24] A mixture containing 45 ml of concentrated nitric acid and 87.5 ml of sulfuric acid was prepared in an ice bath and then graphite flakes (5 g) were added to this mixture. After that, 20 g of potassium chlorate was slowly added to the mixture over 1 hour. After settling for 96 hours, the mixture was diluted with 2000 ml of cold water. The diluted mixture was then washed on a filter with 5% HCl solution and several times with DI water until the solution pH reached neutral. The synthesized graphite oxide was re-dispersed in DI water in an ultrasonic bath for 3 hours to create a 2 wt% dispersion to produce graphene oxide, followed by centrifugation at 4000 rotations per minute for 15 minutes to remove any unexfoliated graphite oxide flakes. GO was reduced chemically using hydrazine to produce chemically reduced graphene oxide (C-RGO). A modified method for the reduction was followed (for more detail, see reference 15). In brief, GO suspension was kept in an ice bath, and 5 mM hydrazine was added drop wise in 20 minutes in order to achieve a slow reduction process. After adding Hydrazine, GO suspension was kept on a hot plate at ~60 °C for an hour. This reduction process avoids aggregation and agglomeration of the flakes because of the controlled kinematics of the reactions.

*Preparation of C-RGO film and CT-RGO:* C-RGO paper was prepared by vacuum filtration of the reduced graphene oxide solution, followed by drying at 60 °C for 1 hour. Prior to preparation of film, chemicals RGO was ultrasonicated in Dimethylformamide (DMF) for 15 minutes and immediately used in film preparation. An electrical device was fabricated to investigate the electronic properties of the drop casted RGO film on Cr (6 nm)/Au (50 nm) electrodes (deposited by e-beam evaporation on a 300 nm thick thermal oxide layer over a p-doped Si chip). The thickness of RGO film was kept submicron range and a channel length was 1.7 mm. RGO paper was kept in a high vacuum chamber ($10^{-6}$ mTorr) and temperature of the

chamber was increased up to 1900 °C to prepare the CT-RGO film. Obtained CT-RGO sample was dispersed in DMF using ultrasonication to cast a film by drop coating method.

*Characterization techniques:* The morphology of the samples was characterized by field-emission scanning electron microscopy (JEOL, Model JSM 7000F). A transmission electron microscopy (JEOL, Model JEM 2100-2100F) at 200 kV for electron beam diffraction and Raman spectroscopy (Witec) with excitation wavelength of 532 nm were used to obtain the structural information. The XPS analysis (QUANTUM 2000, Physical Electronics, USA) was performed using focused monochromatized Al $K_\alpha$ radiation (1486.6 eV) in order to determine changes in the atomic ratios of oxygen to carbon and the existence of functional groups. (see supporting information). The I-V measurements were carried out by two terminal method using a Keithley Source Meter Unit (Model: 237). Low temperature measurements were performed in a pumped $He^4$ cryostat.

## 3. Results and Discussion

### 3.1 I-V measurements at high bias

I-V measurements were performed by two terminal method to investigate the charge transport in RGO film. The optical image of the electrical device and scanning electron micrograph (SEM) of a portion of RGO film are shown in Fig. 1a and b, respectively. Fig. 1c is the schematic diagram of the device. The maximum current was limited to 100 mA to avoid electrical breakdown of the device.

Room temperature (RT = 300 K) I-V measurements of RGO film (Fig. 2a) consists of three distinct responses corresponding to different range of applied source to drain voltages: i) linear response to the applied voltage shaded with sky blue colour and indicated as 'Region (I)' in low bias voltages (below ~±20 V), ii) small deviation from linear response, indicated 'Region (II)' during the intermediate range (up to ~±40V), and iii) a strong non-linear response in 'Region



 

(III)' above a threshold voltage. Thus a current switching of order $10^5$ can be observed on the application of ~0.035 $V\mu m^{-1}$ strength of the electric field as shown Fig. 2b. The variation in the I-V curve corresponding to different applied potential range becomes more obvious in Fig. 2c which shows a graph of differential conductance vs. applied voltage. Up to the threshold voltage, almost a plateau region can be observed, whereas in 'Region (III)', the conductance of the RGO film was increased by a factor ~12 compared to its initial value. Moreover, in Fig. 2a, a hysteresis at high bias region during reverse sweeping of the voltage was also observed. Due to this hysteresis, the maximum conductance value corresponding to the positive and negative biasing shown in Fig. 2c is different. Unlike to 'RGO flake', a sharp increase in the current (switching behaviour) above a threshold voltage ($V_{th}$) ~ ±45 V in I-V curve (Fig. 2a) seems an intriguing feature of the 'RGO film'. For further investigation, low temperature measurements were performed in a pumped He cryostat. Fig. 2d compares I-V curves obtained at three temperatures (4.2 K, 100 K and 300 K). The threshold voltage shifts towards higher value as the temperature of sample decreases while the current switching and hysteresis at higher applied voltages remains. Current saturation seen at very high voltage is due to the compliance current being limited to 100 mA. In Fig. 3a, resistance of the RGO film as a function of temperature (R-T curve) in the range of 10 to 290 K has been shown. The nature of the R-T curve indicates that RGO sample has intrinsic semiconductor character with some metallic contribution.

In the presence of disorder or impurities, the charge carriers spend more time in localized states and consequently the charge transport can be realized either via hopping or via quantum tunnelling of carrier charges between these localized states. Under low bias and in a single flake of chemically RGO the charge transport was found to be consistent with the 2D-VRH model.[11,12] Although our sample shows nonlinear resistance, the VRH model does not provide a good fit to our data even for a very small applied voltage (70 mV) as plotting the logarithm of the resistance

as a function of $(1/T)^n$ with n = 1/3 for 2D or 1/4 for 3D, we obtain nonlinear dependencies as shown in Fig. 3b and c, respectively. Moreover if the energy gained by charge carriers under high bias is larger than the average hopping energy, the VRH model would not be applicable.[25] Fig. 3d shows that RGO does not form any Schottky barrier with gold as the Schottky effect plot is not linear. Basically chemically exfoliated graphene from graphene oxide, especially without any annealing or plasma treatment, forms ohmic contact with gold[26] imply that the origin of this behaviour does not arise from the graphene-gold contact. Therefore we have to look an appropriate mechanism to explain transport behaviour in our RGO film and that should be consistent in all three regions shown in Fig. 2a.

### 3.2 The distributed tunnel junction network

To find out the nature and amount of present impurities, chemically RGO sample was characterized by X-ray Photoelectron Spectroscopy (XPS) and compared with GO sample (Fig. 4). A considerable amount of remnant oxygen-bearing functional groups in RGO was confirmed from the elemental analysis obtained by the XPS which is presented in Table 1. The deconvoluted peaks of C1s in Fig. 4b (of GO) and d (of C-RGO) show that these oxygen bearing functional groups are mainly due to the presence of C-H(C-C, C=C), C-OH (hydroxyl), (C-O-C) epoxide, C=O (carbonyl C), and O=C-OH (carboxylate C) functional groups.[5,13,14] The presence of similar deconvoluted peaks can be observed in the XPS of C-RGO sample, and thus significant portion in the chemically RGO film could be electrically insulating in nature. The size and distribution of these insulating sites can be estimated using high resolution HRTEM and Raman spectroscopy.

Fig. 5 shows high resolution transmission electron micrographs (HRTEM) of a flake of chemically RGO. A careful observation of micrograph reveals the presence of insulating remnants regions (region enclosed by red dotted lines) surrounded by the ordered carbon (crystalline graphene). In the electron beam diffraction pattern of RGO sample (inset of Fig. 5a), a set of



 

distinguishable hexagons can be observed. Such a set of hexagons is generally attributed to the presence of a few layers of graphene stacked in different orientations due to the reduced interlayer interactions originating from the chemical oxidation and reduction processes.[27] Whereas in the case of well interacting layers (stacked in a certain order, Bernal or rhombohedral) instead of hexagon points, circular ring would be observed. The electron beam diffraction of the flake is consistent with HRTEM image where different orientation of crystalline graphene from the same flake shown in Fig. 5b (covered with white dotted regions) can be observed. Similar observations about the atomic and chemical structure of RGO has been reported.[4,9,13,14,28-30] Several reports claim that graphite oxide has amorphous nature but reports on TEM study of the graphite oxide refletc that it has an ordering, similar to graphite.[27,31-32] Therefore, although the reduction and oxidation process involves incorporation of defects and dislocations contribute as a disorder, whereas the remnants oxygen bearing functional groups serve as insulating area, rather as a disordered area. Moreover because of the oxidation and reduction process, flake to flake and interlayer layer interaction would be very weak.

To obtain detail structural distributions in RGO film, it was further characterized by confocal Raman spectroscopy (Fig. 6a-d) using 532 nm excitation wavelength. A large variation in its structure was observed through the mapping (10×10 $\mu m^2$ area) of the RGO film. Fig. 6a shows the representative Raman spectra in two extreme reduction conditions: highly reduced region (HRR) and lightly reduced region (LRR). The D-band originating from the disorder and graphene edges was observed around 1350 $cm^{-1}$ in both the Raman spectra. Fig. 6b shows the position of G-band (originating from the tangential vibration) was centered at 1579 $cm^{-1}$ in highly reduced RGO and position was significantly shifted in the lightly reduced RGO (~13 $cm^{-1}$ shift) due to the decrease of remnant oxygen functional groups. On the other hand, D-band to G-band intensity ratio ($I_D/I_G$) in lightly reduced region was almost doubled (from 0.75 to 1.56). It is

surprising that even after the reduction of GO, the $I_D/I_G$ ratio increases, similar to that what others also observed.[33-35] The exact reason behind it is not clear yet but we believe that the presence of the edges and distributed insulating regions throughout the sample give rise increased backscattering of phonons with defects leads to increase in $I_D/I_G$ ratio.[34,35] A comprehensive distribution of highly and lightly reduced regions in RGO films was observed by confocal Raman mapping of the G-band position and $I_D/I_G$ ratio shown in Figs. 6c and d, respectively. Thus nano-sized distributed insulating remnants are surrounded by crystalline graphene.[4,13,14] The presence of insulating remnants in the matrix of crystalline graphene (well reduced portion of GO) and a very weak interaction between adjacent layer act as a potential barrier against the charge transport. Therefore RGO film appears as the nano-sized remnant insulating area are randomly distributed in the matrix of crystalline graphene forming distributed tunnel junction network. In this situation, initially during very low bias a small contribution from the hopping conduction could be occurred, but at higher bias quantum tunnelling could be more dominant. In this context the generalized theory for quantum tunnelling given by Simmons[17] that covers a range of applied potential could be an adequate model to explain the charge transport mechanism in RGO film. But this theory is applicable to a single tunnel junction. Therefore to explain the charge transport behaviour in a distributed single tunnel junction network, incorporation of additional parameters to Simmons generalized theory is required which is explained as follows.

The distributed tunnel junction network can be assumed to have a set of equivalent parallel and series channels of tunnel junctions. Therefore, the applied voltage between the source and drain will be distributed over the number of individual tunnel junctions in series. Consequently the effective bias on individual tunnel junction would be much less than the applied voltage between the source and drain. Similarly, the current obtained between source and drain will be sum of the currents flowing through the equivalent parallel channels of the film. If there are $n_1$



 

equivalent parallel channels then to describe a chemically RGO film as a distributed tunnel junction network, we define the measured current I as,

$$I = \sum_{1}^{n_1} \left\{ \left(\emptyset - \frac{ev}{2}\right) exp\left[ -\frac{4\pi s}{h}(2m)^{\frac{1}{2}}\left(\emptyset - \frac{ev}{2}\right)^{\frac{1}{2}} \right] - \left(\emptyset + \frac{ev}{2}\right) exp\left[ -\frac{4\pi s}{h}(2m)^{\frac{1}{2}}\left(\emptyset + \frac{ev}{2}\right)^{\frac{1}{2}} \right] \right\} \quad (1)$$

where $\boldsymbol{v=V/n_2}$ (2)

is the effective potential on individual junctions, $V$ is the applied bias between source and drain, $s$ is the thickness of the insulating layer, $\emptyset$ is the barrier height, $m$ is the electron mass, $e$ is the electron charge. Equation (1), is a modified Simmons' equation, expresses the tunneling current through a rectangular barrier in a distributed tunnel junction network. Thus applied bias would be divided over the number of tunnel junctions in series and the total current constitute by adding current through all parallel channel junctions given by equation (1). The modified Simmon's equation (1), includes two fitting parameters of $n_1$ and $n_2$, depend on the distribution of tunnel junctions, and represent the average number of equivalent parallel current channels and the average number of series junction barriers, respectively.

Under extremely low bias ($v \cong 0$) the Simmons equation is modified to

$$I \propto \sum_{1}^{n_1} v\, exp\left(-\frac{4\pi s\sqrt{2m\emptyset}}{h}\right) \quad (3)$$

In this limit the current is directly proportional to the voltage, consistent with our observation of a linear response up to ~ 20 V (Region I, Fig. 2a). Increase in potential between source and drain will gradually increase the potential drop across the individual tunnel junction and follow the equation (1) provided that applied potential $v < \emptyset_B/e$. Accordingly during this range of applied voltage a deviation from linearity in the I-V curve will be observed (Region II, Fig. 2a).

Moreover, if further increase in applied potential falls in the condition $v > \emptyset_B/e$ on individual junction, the electron transport phenomenon would be governed by the F-N tunneling where electrons are able to cross easily the vacuum level (barrier height) of the junction due to its bending and corresponding voltage dependence of the current is given as[17,36,37]

$$I \propto \sum_{1}^{n_1} v^2 exp\left(-\frac{8\pi s\sqrt{2m\emptyset^3}}{2.96ehv}\right) \quad (4)$$

Thus the I-V curve in F-N region should deviate considerably from the linearity (Region III, Fig. 2a) due to the narrowing of the barrier height as its shape changes from rectangular to triangular in the presence of high applied potential. If observed current switching is associated with F-N tunneling, a linear F-N plot (a graph $\ln(I/V^2)$ vs. $1/V$) should be observed. To verify this, F-N plot corresponding to different temperatures was plotted in Fig. 7a. The negative slopes were obtained at high voltage region, confirming F-N tunneling behavior among adjacent junction tunneling barriers. By expanding F-N plot to a wider range of voltages, a clear transition from F-N to direct tunneling region was observed in voltage and temperature space (Fig. 7b) that confirms the validity of generalized theory of Simmons for our sample. Recently similar transition of tunneling transport in single tunnel junction has been reported by a few researchers in other materials.[18-20] But the appearance of this kind of transition in RGO film shows its intriguing properties and strengthen the concept of distributed tunnel junction, as the inter-electrode (source to drain distance) was kept at 1.7 mm and eliminate the probability of tunneling between the electrodes. Moreover, the threshold voltage corresponding to current switching in Fig. 2a was well manifested as a transit line from direct to F-N tunneling shown in Fig. 7b. This implies that at higher applied voltage, charge carriers can easily traverse through the sample because of narrowing of barrier potential. The experimental I-V curve of RGO that falls within the criteria of the direct tunneling was fitted using the equation (1) to get the parameters of the statistically



 

distributed individual tunneling junctions network (Fig. 7c). The fitted curve is consistent with the equation (3), where the I-V curve shows almost linear behavior in the very low effective bias region ($v \cong 0$) following a deviation from linearity according to equation (1) with parameters $n_1 \cong 1 \times 10^{10}$ and $n_2 \cong 500$, and the barrier height $\emptyset \cong 0.22$ eV. As obtained from the fitting parameter $n_2$, the average drop of the potential at the junction is around 0.1 V when applied potential was ~50 V. Since the length of the barrier is nm range, the order of effective electric field on the junction would be ~0.1 $Vnm^{-1}$ or $10^6$ $Vcm^{-1}$. This value of the electric field is sufficient to cause F-N tunneling. Moreover, the e-beam diffraction pattern of the RGO flake reveals that even interaction between adjacent layers is very weak due to the presence of oxygen bearing functional group as they functionalize C atom perpendicular to basal plane. Therefore, similar or weaker interaction would exist among adjacent flake to flake contact too. Therefore the possibility of conduction via percolation due to the flake to flake interaction is very low. But there might be contribution in current from the interflake tunneling of charge carriers via these insulating functional groups. This type of tunneling generally governed by the fluctuation induced tunneling which occurs at low bias and thermal induced tunneling at high bias but the contribution from this will be very small because of the applied voltage direction.[38]

### 3.3 Origin of the hysteresis

To investigate the origin of the hysteresis in the I-V curve (Fig. 2a and c), the temperature of the sample was monitored during the measurements. It was found that a significant amount of the heat dissipation occurred due to the local Joule heating, leading to increase in the sample temperature up to 30-40 K during high bias. Similar hysteresis and an increase in temperatures at high bias were observed at low temperatures, down to 4.2 K (Fig. 2c). Therefore, the hysteresis phenomena cannot be ascribed to adsorption-desorption associated charge traps, because oxygen-bearing functional groups in RGO such as epoxy and hydroxyl groups can only be desorbed

above ~473 K. But increase in the temperature due to the Joule heating under high bias results in a significant change in the resistance (see Fig. 3a). This change in resistance can be observed clearly in the Fig. 2b. Therefore the local joule heating could lead to the formation of a hysteresis during the reverse voltage sweep, similar to that observed in magnetite samples.[39]

### 3.4 Role of remnant oxygen bearing functional groups

To confirm the role of remnant oxygen bearing functional groups in electron transport, C-RGO was step wise annealed at 1900 °C in high vacuum ($10^{-6}$ mbar) for an hour to remove all the impurities comprised during the oxidation and reduction process. The XPS analysis of thus obtained chemically and thermally reduced GO (CT-RGO) samples reveals less than 1% oxygen content (Fig. 8a, Table 1). I-V measurements of the CT-RGO film at room temperature reflect the absence of the switching behavior, followed by a Joule breakdown around 48 V (Fig. 8b). A larger conductance (~40 $mAV^{-1}$, Fig. 8c) was observed compared to C-RGO sample due to the presence of defects and disorder in CT-RGO sample and hardly any oxygen bearing functional groups. To get a clearer idea, powder x-ray diffraction (XRD) and Raman spectroscopy of samples were carried out. Fig. 8d shows the XRD chemically RGO and CT-RGO films. The XRD of these two samples clearly indicates that during the thermal annealing of the C-RGO at 1900 °C, graphitization of the sample occurred due to the removal of oxygen bearing functional groups and favoring a strong interaction among the adjacent layers because of reduced interlayer distance. This excludes the possibility of any sorts of tunneling within the film. However, considerable order of defects and disorder can be observed in its Raman and XRD spectrum and due to this, a nonlinear I-V characteristic was observed.

## 4. Conclusions

In conclusion, charge transport in a chemically RGO film was studied under high bias. The I-V curve of a chemically produced RGO film has three distinct responses corresponding to the



 

different range of voltages. Moreover, a current switching of order $10^5$ was observed above a threshold voltage, which was explained as a transition from direct to F-N tunneling. The charge transport mechanism was consistent with quantum tunneling and can be explained using modified Simmons generalized theory in a distributed tunnel junction. Chemically produced RGO film can be considered as distributed tunnel junction network due to the presence of the significant amount of the remnants insulating oxygen bearing function groups in the form of islands and very weak interaction between the adjacent layers. Therefore the presence of these insulating oxygen-bearing functional groups leads to a quantum tunneling-based electron transport in the RGO film. The observation of the hysteresis in the I-V curve at higher bias was explained by Joule heating. Presence of oxygen bearing functional groups plays a key role in charge transport as the transition in transport and current switching behavior were absent when all remnants oxygen-bearing functional groups were stripped away from the sample.

## Acknowledgments

This research was supported by the WCU (World Class University) program (R31-2008-000-10029-0 and R32-2008-000-10204-0), through the National Research Foundation of Korea (NRF) funded by the Ministry of Education, Science and Technology, Republic of Korea.

## Notes and References

[a]WCU Department of Energy Science, Sungkyunkwan University, Suwon 440-746, Republic of Korea

E-mail: sivaram.arepalli@gmail.com

[b]Department of Electrical Engineering, University of California Los Angeles, CA 90095 United States

[c]BK21 Department of Physics, Sungkyunkwan University, Suwon 440-746, Republic of Korea

[d]Laboratoire Interdisciplinaire Carnot de Bourgogne, CNRS-UMR 6303, Université de Bourgogne, Dijon 21078, France

[e]School of Electronic & Electrical Engineering, College of Information & Communication Engineering and SKKU Advanced Institute of Nanotechnology, Sungkyunkwan University, Suwon 440-746, Republic of Korea

[†] S. Pandey and C. Biswas contributed equally to this work.

1 K. S. Novoselov, A. K. Geim, S. V. Morozov, D. Jiang, Y. Zhang, S. V. Dubonos, I. V. Grigorieva, A. A. Firsov, *Science* 2004, **306**, 666.

2 A. H. Castro Neto, F. Guinea, N. M. R. Peres, K. S. Novoselov, A. K. Geim, *Rev. Mod. Phys.* 2009, **81**, 109.

3 S. Stankovich, D. A. Dikin, G. H. B. Dommett, K. M. Kohlhaas, E. J. Zimney, E. A. Stach, R. D. Piner, S. T. Nguyen, R. S. Ruoff, *Nature* 2006, **442**, 282.

4 C. Mattevi, G. Eda, S. Agnoli, S. Miller, K. A. Mkhoyan, O. Celik, D. Mastrogiovanni, G. Granozzi, E. Garfunkel, M. Chhowalla, *Adv. Funct. Mater.* 2009, **19**, 2577.

5 Y. Zhu, S. Murali, W. Cai, X. Li, J. W. Suk, J. R. Potts, R. S. Ruoff, *Adv. Mater.* 2010, **22**, 3906.

6 R. R. Nair, P. Blake, A. N. Grigorenko, K. S. Novoselov, T. J. Booth, T. Stauber, N. M. R. Peres, A. K. Geim, *Science* 2008, **320**, 1308.

7 K. P. Loh, Q. Bao, G. Eda, M. Chhowalla, *Nat. Chem.* 2010, **2**, 1015.

8 S. Stankovich, D. A. Dikin, R. D. Piner, K. A. Kohlhaas, A. Kleinhammes, Y. Jia, Y. Wu, S. T. Nguyen, R. S. Ruoff, *Carbon* 2007, **45**, 1558.

9 I. Jung, D. A. Dikin, R. D. Piner, R. S. Ruoff, *Nano Lett.* 2008, **8**, 4283.

10 G. Eda, C. Mattevi, H. Yamaguchi, H. Kim, M. Chhowalla, *J. Phys. Chem. C* 2009, **113**, 15768.

11 C. Gómez-Navarro, R. T. Weitz, A. M. Bittner, M. Scolari, A. Mews, M. Burghard, K. Kern, *Nano Lett.* 2007, **7**, 3499.

12 A. B. Kaiser, C. Gómez-Navarro, R. S. Sundaram, M. Burghard, K. Kern, *Nano Lett.*



 

2009, **9**, 1787.

13 K. Erickson, R. Erni, Z. Lee, N. Alem, W. Gannett, A. Zettl, *Adv. Mater.* **2010**, *22*, 4467.

14 C. Gómez-Navarro, J. C. Meyer, R. S. Sundaram, A. Chuvilin, S. Kurasch, M. Burghard, K. Kern, U. Kaiser, *Nano Lett.* **2010**, *10*, 1144.

15 T. Ghosh, C. Biswas, J. Oh, G. Arabale, T. Hwang, N. D. Luong, M. Jin, Y. H. Lee, J.-D. Nam, *Chem. Mater.* **2012**, *24*, 594.

16 P.-G. Ren, D.-X. Yan, X. Ji, T. Chen, Z.-M. Li, *Nanotechnology* 2011, **22**, 055705.

17 J. G. Simmons, *J. Appl. Phys.* 1963, **34**, 2581.

18 J. M. Beebe, B. Kim, J. W. Gadzuk, C. Daniel Frisbie, J. G. Kushmerick, *Phys. Rev. Lett.* 2006, **97** 026801.

19 Q. Lu, K. Liu, H. Zhang, Z. Du, X. Wang, F. Wang, *ACS Nano* 2009, 3, 3861.

20 W. Fan, J. Lu, S. A. Wolf, *Appl. Phys. Lett.* 2010, **97**, 242113.

21 A. Asamitsu, Y. Tomioka, H. Kuwahara, Y. Tokura, *Nature* 1997, **388**, 50.

22 Y. Watanabe, J. G. Bednorz, A. Bietsch, C. Gerber, D. Widmer, A. Beck, S. J. Wind, *Appl. Phys. Lett.* 2001, **78**, 3738.

23 S. Lee, A. Fursina, J. T. Mayo, C. T. Yavuz, V. L. Colvin, R. G. S. Sofin, I. V. Shvets, D. Natelson, *Nature Mater.* 2007, **7**, 130.

24 L. Staudenmaier, *Ber. Dtsch. Chem. Ges.* 1898, **31**, 1481.

25 G. G. Raju, *Dielectrics in Electric Fields*. Marcel Dekker Inc.: NewYork, United States of America, 2003, Ch. 7.

26 R. S. Sundaram, C. Gomez-Navarro, E. J. H. Lee, M. Burghard, K. Kern, *Appl. Phys. Lett.* 2009, **95**, 223507.

27 N. R. Wilson, P. A. Pandey, R. Beanland, R. J. Young, I. A. Kinloch, L. Gong, Z. Liu, K. Suenaga, J. P. Rourke, York, S. J. Sloan, *ACS Nano* 2009, **3**, 2547.

28 K. A. Mkhoyan, A. W. Contryman, J. Silcox, D. A. Stewart, G. Eda, C. Mattevi, S. Miller, M. Chhowalla, *Nano Lett.* 2009, **9**, 1058.

29 G. Wang, J. Yang, J. Park, X. Gou, B. Wang, H. Liu, J. Yao, *J. Phys. Chem. C* 2008, **112**, 8192.

30 J. I. Paredes, S. Villar-Rodil, P. Solis-Fernandez, A. Martinez-Alonso, J. M. D. Tascon, *Langmuir* 2009, **25**, 5957.

31 F. A. De La Cruz, J. M. Cowley, *Nature* 1962, **196**, 468.

32 F. A. De La Cruz, J. M. Cowley, *Acta Crystallogr.* 1963, **16**, 531.

33 H. K. Jeong, Y. P. Lee, R. J. W. E. Lahaye, M.-H. Park, K. H. An, I. J. Kim, C.-W. Yang, C. Y. Park, R. S. Ruoff, Y. H. Lee, *J. Am. Chem. Soc.* 2008, **130**, 1362.

34 D. R. Dreyer, S. Park, C. W. Bielawski and R. S. Ruoff, *Chem. Soc. Rev.* 2010**, 39**, 228.

35 L. M. Malarda, M. A. Pimentaa, G. Dresselhaus, M. S. Dresselhaus, Phys. Rep. 2009, **473**, 51.

36 S. Pandey, P. Rai, S. Patole, F. Gunes, G.-D. Kwon, J.-B. Yoo, P. Nikolaev, and S. Arepalli, *Appl. Phys. Lett.* 2012, **100**, 043104.

37 K. L. Jensen, *Vacuum microelectronics (Ed: Wei Zhu)* Wiley-Interscience Publication: 2001, Ch. 3.

38 M. Salvato, M. Cirillo, M. Lucci, S. Orlanducci, I. Ottaviani, M. L. Terranova, F. Toschi, *Phys. Rev. Lett.* 2008, **101**, 246804.

39 A. A. Fursina, R. G. S. Sofin, I. V. Shvets, D. Natelson, *Phys. Rev. B* 2009, **79**, 245131.



 

**Fig. 1** (a) Schematic diagram (in inset optical image) of chemically RGO film based device. (b) Scanning electron micrograph of a portion of the film.

**Fig. 2** (a) I-V curve of RGO film at 300 K, the direction of arrows indicates the direction of the voltage sweeping. Schematics are the shape of barrier potential under various ranges of applied voltage. (b) Semilogarithmic plot of I-V curve and (c) differential conductance of the RGO film at 300 K. (d) The I-V curve corresponding to 300 K, 100 K and 4.2 K. The saturation in the I-V curves is observed due to the setting compliances current for 100 mA.

**Fig. 3** (a) Temperature dependence resistance of the RGO film.. Semilogarithmic plot of current (b) 2D VRH model (against $T^{-1/3}$) and (c) 3D VRH model (against $T^{-1/4}$); according to the variable range hopping (VRH) model $\boldsymbol{I = I_0 e^{-(T/T_0)^{1/n}}}$ where I is the current, T is the temperature, n is the dimension of the sample, $\boldsymbol{I_0}$ and $\boldsymbol{T_0}$ are the constants. (d) Schottky plot of ln(I) vs. $V^{1/2}$.

**Fig. 4** (a) Full range XPS spectrum and (b) deconvoluted C1s peak of GO film. (c) Full range XPS spectrum and (d) deconvoluted C1s peak of RGO film.

**Fig. 5** (a) and (b) HRTEM images of a portion of RGO flake. White dotted enclosed region is the crystalline graphene and red colours enclosed are the remnant functionalized portion of graphene. Inset is the e-beam diffraction pattern of a RGO flake. (b) Shows the presence of multilayers in a flake due to reduced interaction.

**Fig. 6** (a) A comparative Raman spectra normalized to G-band of GO and lightly reduced GO and highly reduced GO regions in a chemically RGO film (using 532 nm of excitation wavelength). (b) G-band of GO, lightly reduced GO and highly reduced regions for RGO film imply a systematic reduction in Raman

shift according to the degree of reduction and consequently the presence of the oxygen functional groups. (c) The distribution of G-band position in chemically RGO film mapped in the area of 50 $\mu m^2$ by confocal Raman spectroscopyand (d) D to G-band ratio of the corresponding area.

**Fig. 7** (a) The F-N plot of chemically RGO film in F-N tunneling region. (b) The F-N plot extended to direct tunneling region to show the transition at 300, 100 and 4.2 K temperature. (c) RT modified Simmons equation (equation (1)) fitted I-V curve corresponding to the direct tunneling region with fitted parameters.

**Fig. 8** (a) XPS spectrum of RGO and CT-RGO samples, (b) I-V curve, and (c) differential conductance of CT-RGO film at 300 K. (d) XRD and (e) Raman spectra of C-RGO and CT-RGO samples.

**Table 1:** Comparison of C, O and O/C ratio for GO, chemically RGO, and CT-RGO samples obtained from XPS.

| Sample name | C (atomic %) | O (atomic %) | O/C ratio |
|---|---|---|---|
| **GO** | 73.73 | 25.38 | 0.344 |
| **C-RGO** | 91.5 | 7.6 | 0.083 |
| **CT-RGO** | 99.029 | 0.971 | 0.01 |

## Table of contents entry heading:

A transition from direct to F-N tunnelling is observed in reduced graphene oxide film under wide range of applied potential.



 

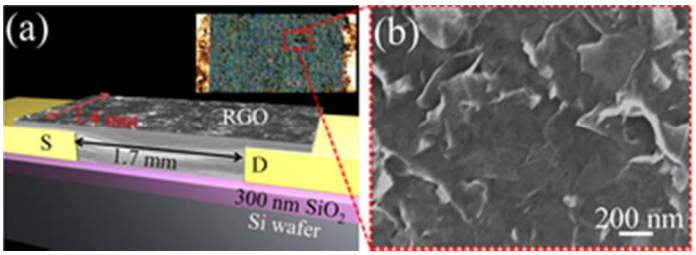


29x10mm (300 x 300 DPI)

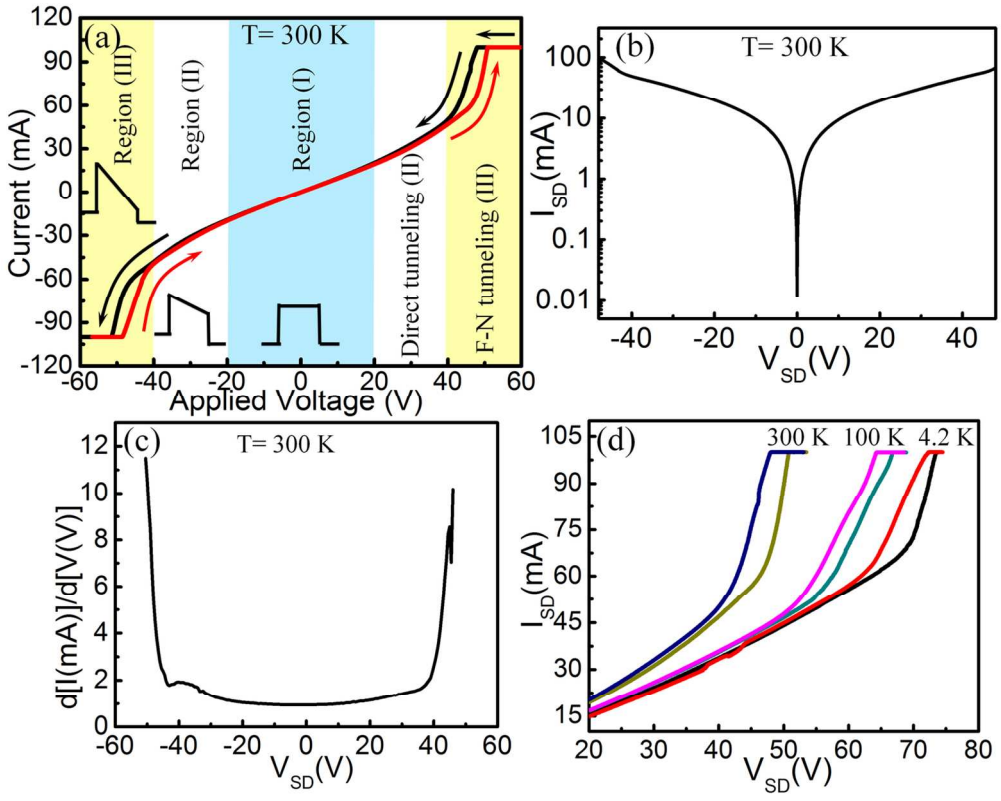


135x107mm (300 x 300 DPI)

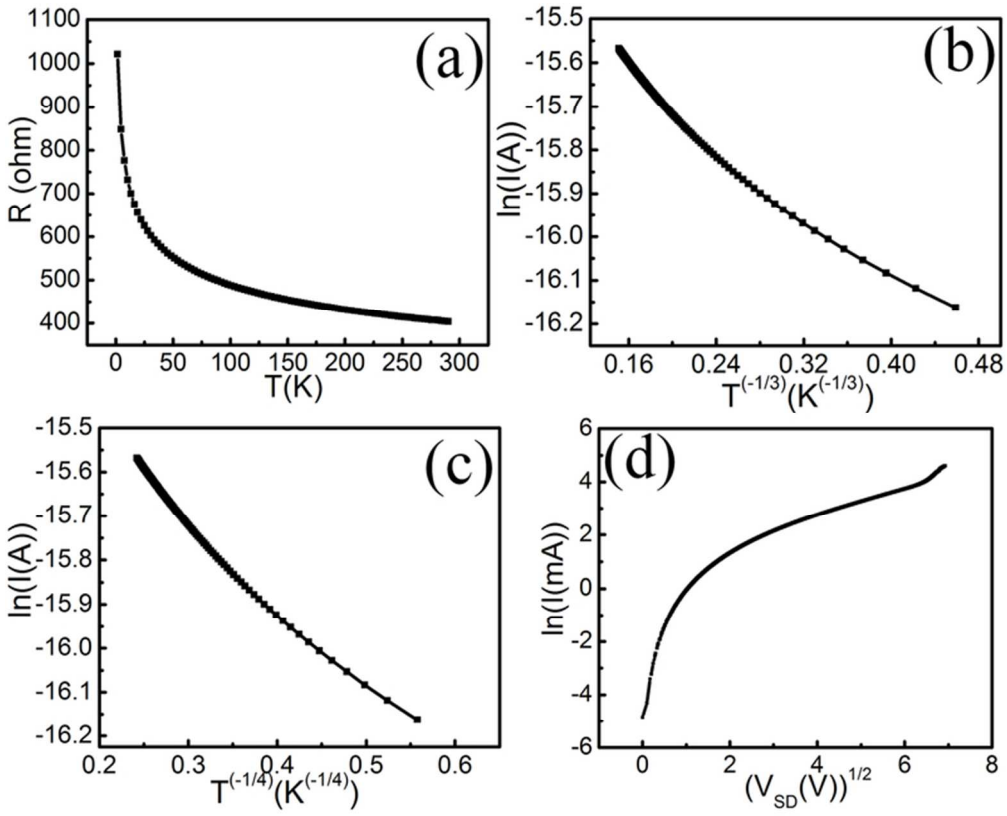


67x55mm (300 x 300 DPI)

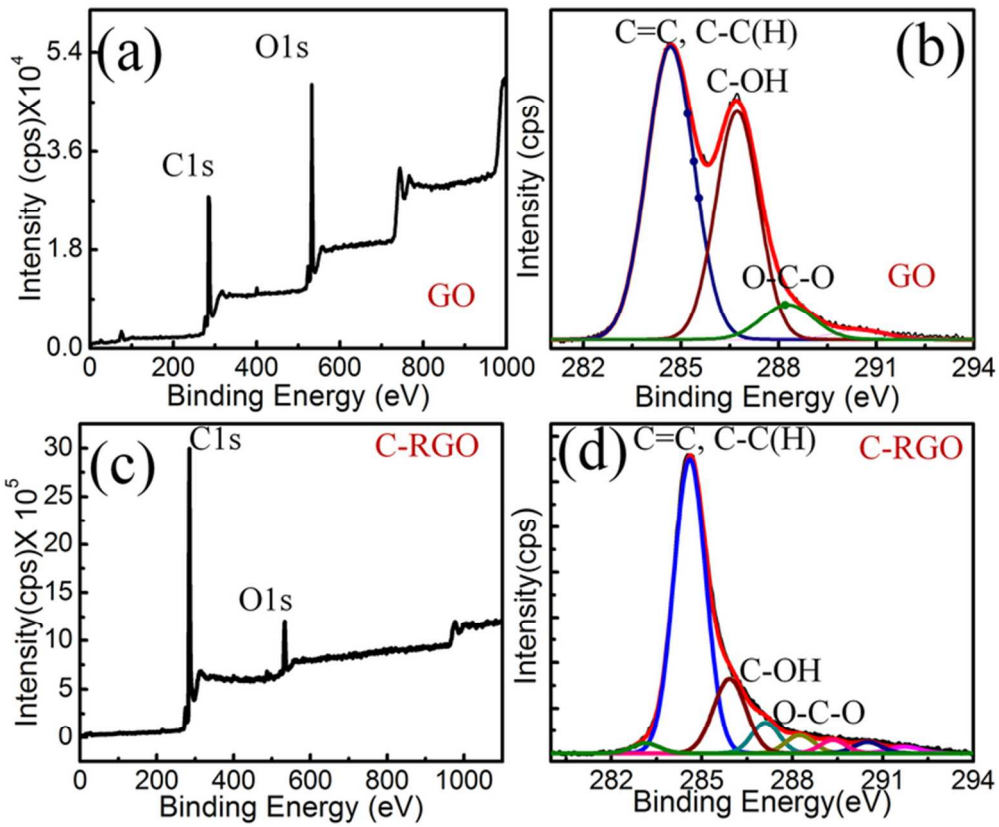


68x56mm (300 x 300 DPI)

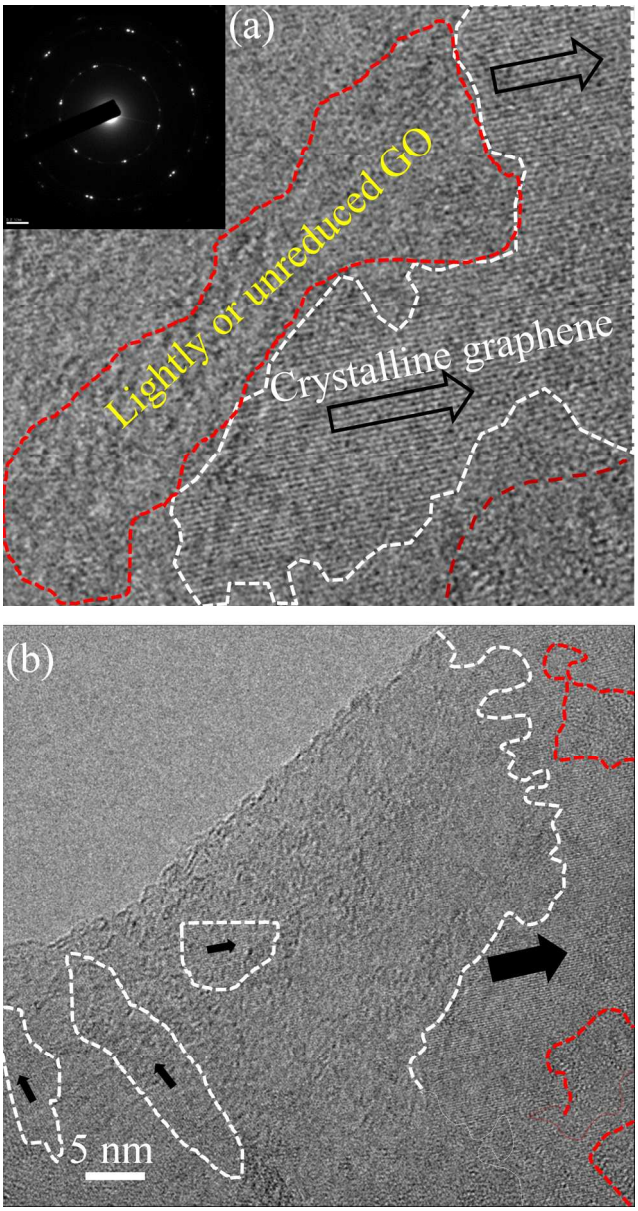


156x297mm (300 x 300 DPI)

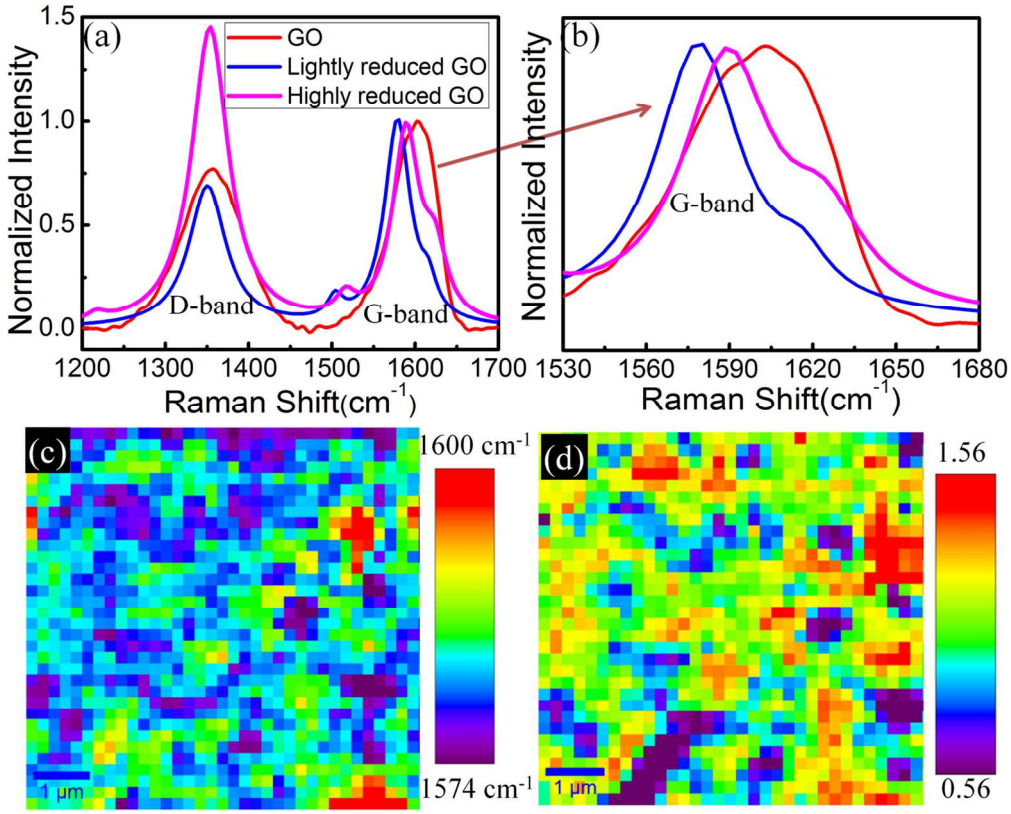


137x110mm (300 x 300 DPI)

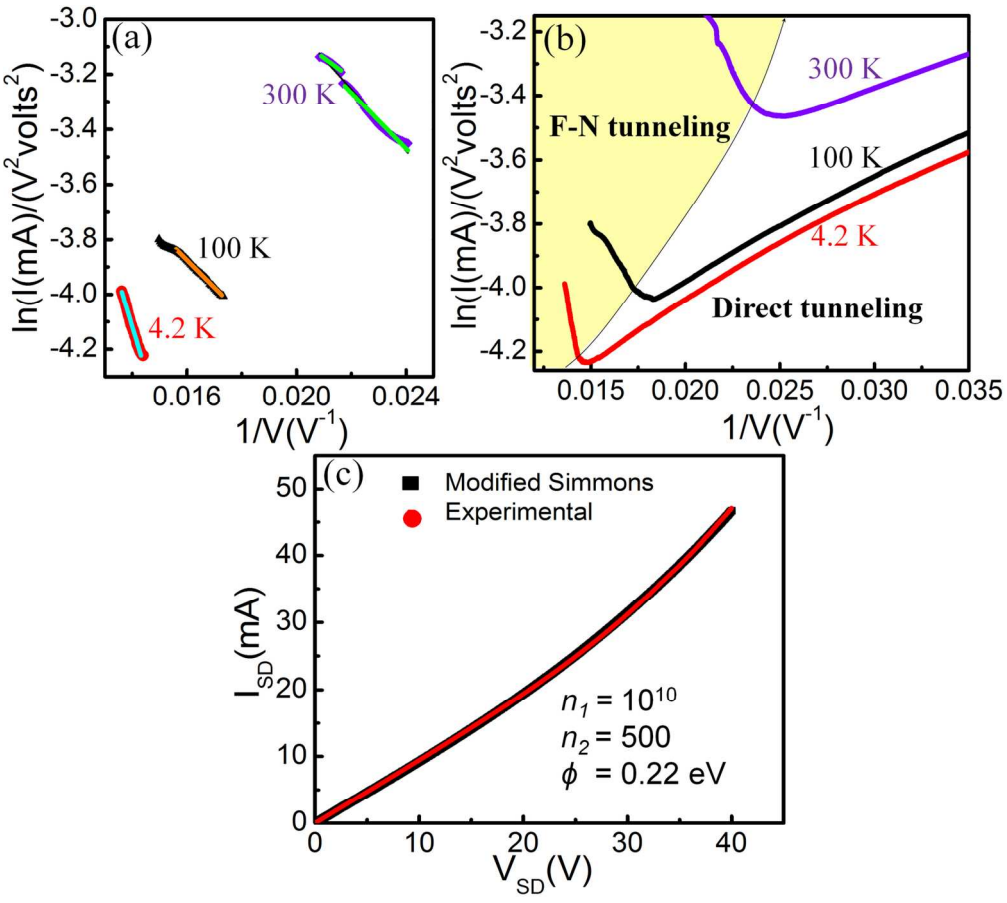


151x134mm (300 x 300 DPI)

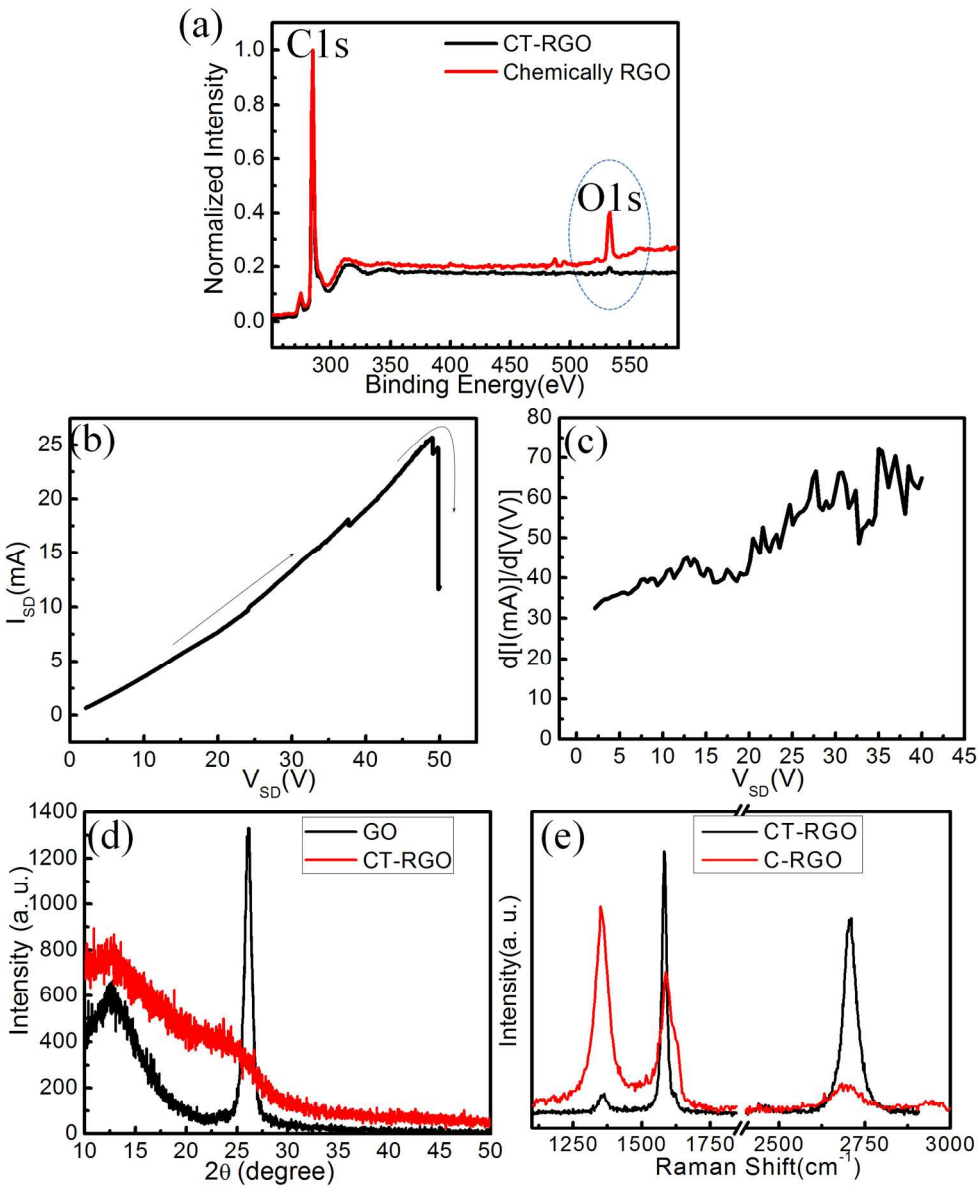


209x257mm (300 x 300 DPI)

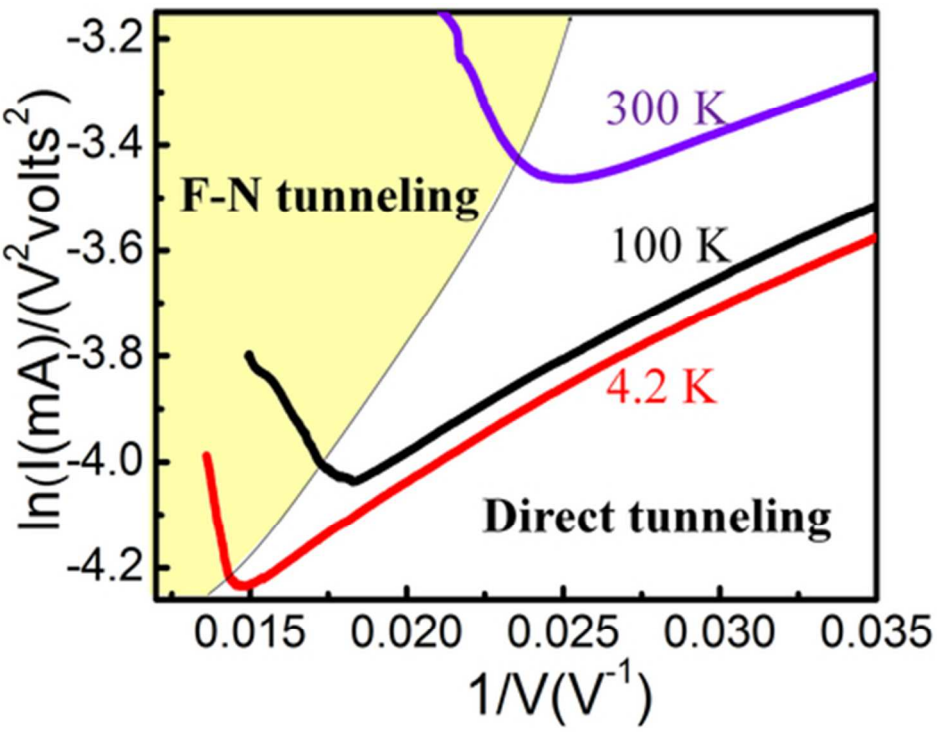


39x30mm (300 x 300 DPI)